NANO LETTERS

Letter

Cite This: Nano Lett. 2019, 19, 3953−3960

pubs.acs.org/NanoLett

Heterogeneous Photon Recycling and Charge Diffusion Enhance Charge Transport in Quasi-2D Lead-Halide Perovskite Films

Silvia G. Motti,[†] Timothy Crothers,[†] Rong Yang,[‡] Yu Cao,[‡] Renzhi Li,[‡] Michael B. Johnston,[†] Jianpu Wang,*[,‡] and Laura M. Herz*[,†]

[†]Department of Physics, University of Oxford, Clarendon Laboratory, OX1 3PU Oxford, United Kingdom

[‡]Key Laboratory of Flexible Electronics (KLOFE) and Institute of Advanced Materials (IAM), Jiangsu National Synergetic Innovation Center for Advanced Materials (SICAM), Nanjing Tech University, 30 South Puzhu Road, Nanjing 211816, China

Supporting Information

ABSTRACT: The addition of large hydrophobic cations to lead halide perovskites has significantly enhanced the environmental stability of photovoltaic cells based on these materials. However, the associated formation of two-dimensional structures inside the material can lead to dielectric confinement, higher exciton binding energies, wider bandgaps and limited charge-carrier mobilities. Here we show that such effects are not detrimental to the charge transport for carefully processed films comprising a self-assembled thin layer of quasi-two-dimensional (2D) perovskite interfaced with a 3D $MAPbI_3$ perovskite layer. We apply a combination of time-resolved photoluminescence and photoconductivity spectroscopy to reveal the charge-carrier recombination and transport through the film profile, when either the quasi-2D or the 3D layers are selectively excited. Through modeling of the recorded dynamics, we demonstrate that while the charge-carrier mobility is lower within the quasi-2D region, charge-carrier diffusion to the 3D phase leads to a rapid recovery in photoconductivity even when the quasi-2D region is initially photoexcited. In addition, the blue-shifted emission originating from quasi-2D regions overlaps significantly with the absorption spectrum of the 3D perovskite, allowing for highly effective "heterogeneous photon recycling". We show that this combination fully compensates for the adverse effects of electronic confinement, yielding quasi-2D perovskites with highly efficient charge transporting properties.

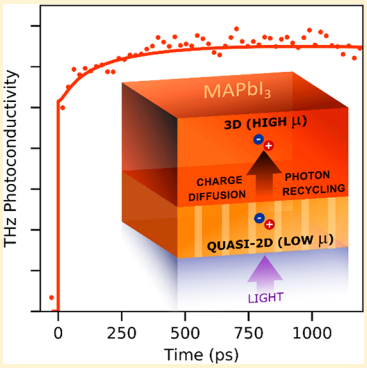

KEYWORDS: *Solar cells, charge-carrier dynamics, mobility, hybrid perovskites, photon reabsorption, nanostructured*

Metal halide perovskite semiconductors have recently emerged as promising materials for photovoltaic devices, whose efficiencies have reached over 23%.[1] However, a significant obstacle to commercial application is the poor stability of this class of materials, in particular upon exposure to moisture.[2−4] One strategy to overcome this challenge is the addition of large hydrophobic organic cations to the perovskite precursors as part of the film fabrication process, which has proven to enhance the moisture resistance and the environmental stability of the material.[5,6] Since these molecules are too large to fit into the perovskite octahedra, they instead form interlayers that induce the formation of a two-dimensional (2D) structure. While these hydrophobic spacers thus reduce moisture permeability, they also form a dielectric barrier between adjacent layers of the metal halide perovskite. Such dielectric confinement may result in higher exciton binding energies, wider bandgap, and limited charge-carrier diffusion lengths[7,8] which are unfavorable characteristics for photovoltaic applications.

To mitigate the adverse effects of charge confinement upon the addition of hydrophobic molecules, quasi-2D compositions have been fabricated for which the ratio between the small cation incorporated into the perovskite lattice and the large hydrophobic cation is carefully tuned. Depending on the exact processing conditions, the resulting films contain various distributions of n semiconducting perovskite layers, and consequently different levels of electronic confinement. In addition, hydrophobic interlayers may be placed in a random or gradient (low to high n) arrangement across the film depth. Such mixed-phase materials can combine the enhanced stability of 2D perovskites with the superior charge-transport properties of their 3D counterpart, as has been demonstrated by their successful implementation in light-emitting diodes[9−12] and photovoltaic devices.[13−20]

Many fundamental and practical questions arise from the presence of such chemical and electronic heterogeneity inside these mixed-phase perovskites. For instance, it has recently been explored how the nature of charge-carriers and their interaction with the lattice differ from what is encountered in the more conventional bulk 3D perovskite semiconductors.[7,8,21−23] For the optimized operation of electronic devices, knowledge of how energy and charge transfer occur between different domains within mixed-phase materials is particularly

Received: March 26, 2019
Revised: May 8, 2019
Published: May 9, 2019

DOI: 10.1021/acs.nanolett.9b01242
Nano Lett. 2019, 19, 3953−3960

important. Although a few studies have investigated electronic interactions between neighboring perovskite sheets and short-scale transfer mechanisms,[24−26] an understanding of how these heterogeneities affect charge transport throughout a film's depth is urgently required for optimization of charge conduction on the device scale.

In this study, we address this issue by investigating mixed-phase quasi-2D/3D lead-iodide perovskite films using a combination of time-resolved photoluminescence (PL) and optical-pump terahertz-probe (OPTP) spectroscopy. We demonstrate that for the deployed processing conditions, the film contains a layer of quasi-2D domains on the side interfacing the substrate, and a predominantly 3D region near the outer side of the film. We find that the mobility of charge-carriers inside the quasi-2D region is on average ∼25% lower than for those present in the 3D (bulk) layer of the film. However, this seemingly detrimental effect of low dimensionality appears to be short-lived, as the OPTP dynamics reveals a transient enhancement of photoconductivity over a time scale of ∼1 ns after primarily the quasi-2D region has been photoexcited. By modeling the charge-carrier dynamics in these films, we demonstrate that this photoconductivity boost results from charge-carriers transferring efficiently from quasi-2D regions to 3D layers, where the charge mobility is higher. We show that such transfers are not only aided by charge-carrier diffusion but also by photon recycling of higher-energy photons emitted from the quasi-2D domains that are particularly efficiently recaptured by the absorption profile of the 3D bulk phase. Our findings therefore reveal that the presence of dielectric confinement in such mixed phase films may be far less detrimental to photovoltaic performance than is commonly assumed. In particular, charge-carrier transfer from quasi-2D to 3D domains with higher mobility can be sufficiently rapid to outcompete recombination and is aided by the upshift in emission energy resulting from electronic confinement, which yields particularly effective photon reabsorption by the 3D region. Hence, we find that for suitable film morphology the enhanced stability of 2D perovskites can be combined with the favorable charge-transport properties of 3D semiconductors.

Mixed phase quasi-2D/3D lead iodide perovskite thin films were fabricated on quartz substrates, based on the smaller methylammonium (MA) cation for incorporation into the lead iodide perovskite lattice, and the larger 3-bromobenzylammonium cation as a spacer (3BBA). Full details of the film fabrication and characterization are provided in the SI. A similar film fabrication method has recently been successfully applied to yield active layers for efficient solar cells with a peak power conversion efficiency of 18.2% and excellent stability in moist environment.[6] The morphology of such films can be examined in Figure 1a, which shows the cross-section of a perovskite film recorded through aberration-corrected scanning transmission electron microscope (STEM, see Supporting Information for details). Although the top surface of the film appears homogeneous on the substrate side, elongated crystallites can be identified which are oriented perpendicular to the substrate. Grazing-incidence wide-angle X-ray scattering (GIWAXS) measurements previously performed on such films[6] have revealed that the outer surface is constituted mostly by 3D $MAPbI_3$ crystallites, while additional peaks associated with 2D-phase perovskite could be observed for higher incidence angle (when the full depth of the films was being probed). Moreover, these measurements indicated a

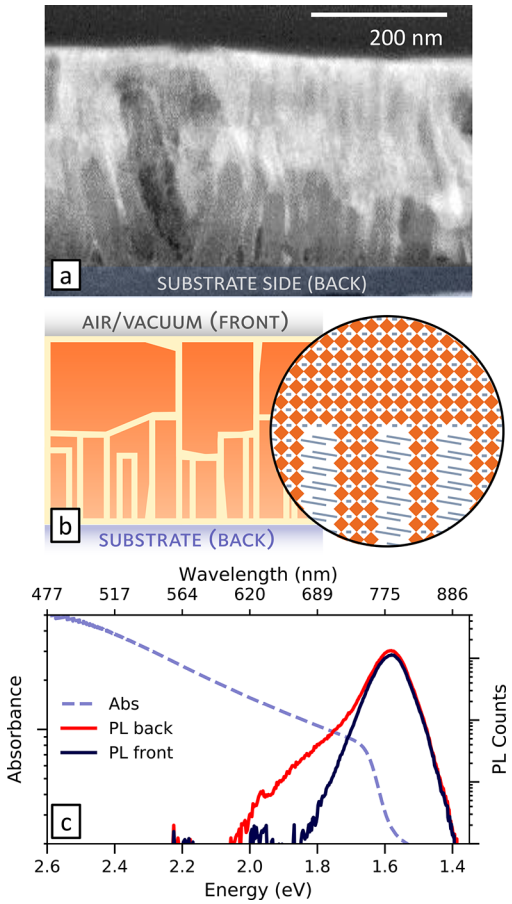

Figure 1. (a) Cross-section of a mixed phase quasi-2D/3D lead iodide perovskite film recorded by STEM (see Supporting Information for details). (b) Schematic illustration of the film morphology showing 3D $MAPbI_3$ crystallites on top and orientated quasi-2D crystallites at the substrate side. (c) Absorption (dashed line, light blue) and PL spectra taken in reflection geometry with excitation at 3.1 eV photon energy either from the front (dark blue) or the back side (red) of the perovskite film.

predominant orientation of the layered structures within the quasi-2D phase perpendicular to the substrate. Previous reports suggest that such preferential formation of quasi-2D domains on the substrate side may be linked to specific parameters such as the solubility of the precursors, the substrate temperature, and surface energies.[7,9−11] On the basis of our experimental evidence, we conclude that the present mixed-phase films comprise two distinct regions, as depicted schematically in Figure 1b. The top layer on the outer surface consists of large 3D $MAPbI_3$ crystallites whereas the substrate-side layer constitutes a blend of smaller 3D crystallites and quasi-2D domains, whose preferential orientation is perpendicular to the film surface.

To probe the optoelectronic properties of each region, we illuminated 450-nm thick films either from the front or the back side with 3.1 eV light and measured the PL spectra in reflection mode (Figure 1c). At this excitation energy, light is strongly absorbed by the lead iodide perovskite with an associated penetration depth shorter than 100 nm (see Figure S2) which means that the initially generated charge-carrier distributions will be located either in the 3D $MAPbI_3$ or the quasi-2D layers. We find that, as expected, front side photoexcitation produces a symmetric narrow-band emission

DOI: 10.1021/acs.nanolett.9b01242
Nano Lett. 2019, 19, 3953−3960

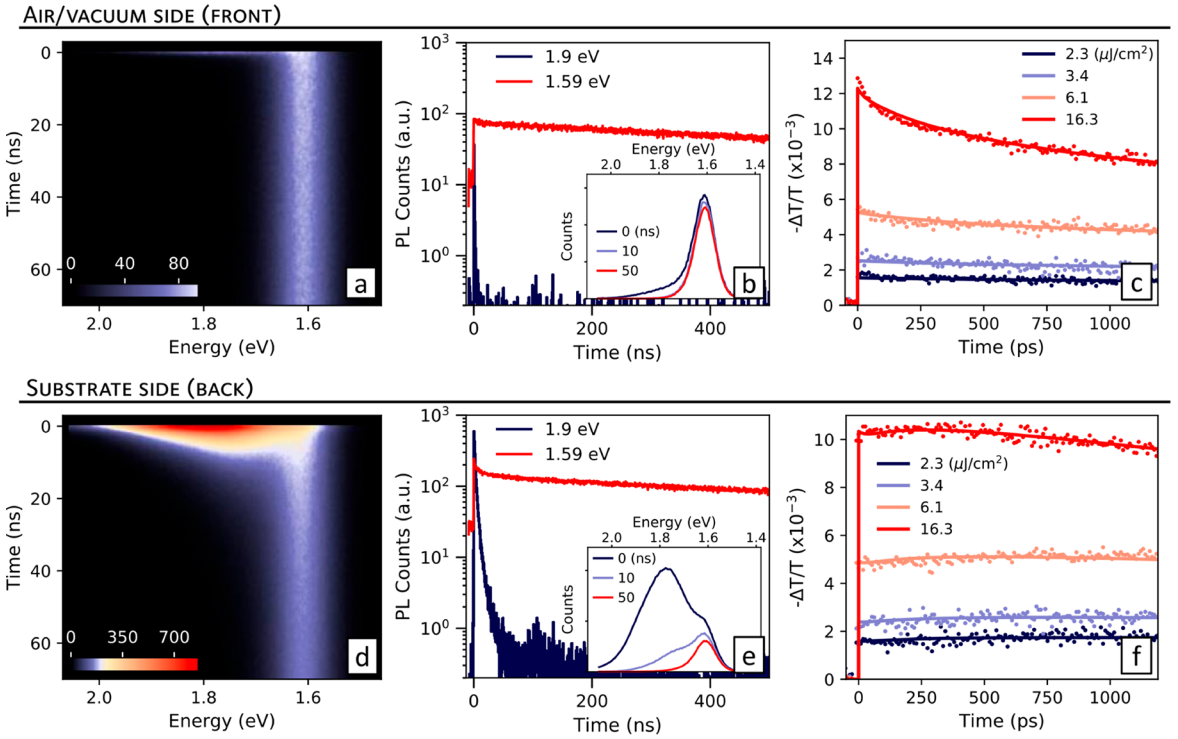

Figure 2. Maps of the time-resolved PL originating from a 3D/quasi-2D lead iodide perovskite film measured in reflection geometry with photoexcitation from the front (a) or the back (d) of the films, taken with an excitation energy of 3.1 eV (500 kHz, fluence ~10 nJ/cm^2); PL decays (point spacing ~3 ns) at 1.59 eV (red) and 1.9 eV (dark blue) taken with photoexcitation from the front (b) or the back (e) of the films; insets show the matching PL spectra at different decay times. OPTP THz photoconductivity transients (plotted as $-\Delta T/T \propto \sigma$; time resolution ~50 fs, excitation at 3.1 eV, repetition rate 5 kHz) taken with photoexcitation incident on the front (c) or back (f) of the films; dots are experimental data points and solid lines are fitted dynamics (which account for charge diffusion and photon reabsorption and assume heterogeneous PL emission).

consistent with conventional 3D $MAPbI_3$ spectra,[27] whereas photoexcitation on the back (substrate side) of the film, however, results in a higher energy shoulder in the emission which is in agreement with the presence of quasi-2D perovskite domains.

To further investigate how the charge-carrier distribution evolves through the film, we measured the PL dynamics following photoexcitation from either the front (Figure 2a,b) or back side of the film (Figure 2d,e). We find that when the film is excited from the back side, the PL spectrum at early times carries the fingerprint of the quasi-2D region, which decays with a lifetime of only 4 ns. This broad-band emission spectrum is superimposed onto the long-lived, narrower emission spectrum of the 3D $MAPbI_3$ region with lifetime >1 μs (see Figure S4 for component analysis). We note that the high-energy emission of the quasi-2D region is centered around 1.74 eV, in contrast to that reported for strongly confined 2D perovskites (n = 1) of similar composition which have exhibited emission in the 2.2−2.5 eV spectral region.[28] In addition, there is no strong presence of sharp higher-energy bandgap phases in the absorption spectrum of the film (Figure 1c, dashed blue line). Although the broad PL emission observed from the present samples does not allow for accurate determination of the n composition, it suggests a predominance of n > 4 quasi-2D domains. The exciton binding energies for such a level of dielectric and electronic confinement are not expected to be so significantly elevated as to be detrimental for photovoltaic applications.[29,30] Nonetheless, even such a low level of confinement apparently has a dramatic effect on the radiative recombination rates of charge-carriers, as evidenced by the high relative intensity and fast decay of the high energy emission originating from the quasi-2D perovskite. Such high emission decay rates could potentially be a limiting factor for photovoltaic devices, where long carrier lifetimes (i.e., long diffusion lengths) are desirable to promote efficient charge extraction. However, these short lifetimes could alternatively be associated with charge and energy transfer dynamics to the lower bandgap domains, which would be beneficial, given that where these are likely to exhibit higher charge-carrier lifetimes and mobilities, and lower exciton binding energies.

To investigate such interplay between confinement effects and the charge transport properties of the mixed-phase films we performed OPTP spectroscopy, which allows us to probe the transient photoconductivity of the film in a contactless manner. The measurements were performed with 3.1 eV pulsed photoexcitation incident either on the front or back of the films, and the transients obtained are shown in Figure 2c,f. The photoinduced differential transmission of terahertz (THz) radiation ($\Delta T/T$) is proportional to the photoconductivity (σ) of the film, which is in turn linearly dependent on the charge-carrier population density and the effective charge-carrier mobility (μ). From the $-\Delta T/T$ amplitude immediately after photoexcitation (i.e., before charge-carrier recombination has occurred), μ can then be extracted under knowledge of the absorbed photon density (see Section 1.5 in Supporting Information for details).[31,32] We find that while photoexcitation from the back side of the film resulted in an initial charge-carrier mobility of 17.4 ± 0.9 cm^2/(V s), this value increased to 23.9 ± 0.9 cm^2/(V s) for excitation from the front

DOI: 10.1021/acs.nanolett.9b01242
Nano Lett. 2019, 19, 3953−3960

side. The ∼25% lower charge-carrier mobility measured when probing the back side of the films is consistent with the presence of quasi-2D domains and the higher concentration of dielectric barriers in this region.[7]

The OPTP measurements further allow us to investigate the subsequent dynamics of charge-carriers following the initial photoexcitation. We note that unlike the PL transients discussed earlier, which tend to overemphasize the contributions from carrier recombination in strongly confined regions that are associated with high radiative efficiencies, the OPTP photoconductivity measurements are particularly sensitive to carriers that are mobile, thus highlighting the electronic response from regions of lower confinement. Figure 2c,f shows that both for back and front side photoexcitation the photoconductivity lifetimes decrease with increasing fluence (for full fluence dependence see Figure S5 in the Supporting Information). This behavior can be described by the typical recombination dynamics of free charge-carriers observed in perovskite semiconductors, which may recombine through a monomolecular trap-assisted mechanism, combined with bimolecular radiative recombination and third order Auger-like processes whose contribution become significant at higher carrier densities.[31,33] At the lowest fluences, transients are generally expected to be flat, as bimolecular and Auger recombination become negligible, and the remaining trap-mediated recombination may occur over a time scale much longer than the observation window of 1 ns. However, while the low-fluence dynamics for front-side excitation of the film indeed appear mostly flat, the transients taken after photoexcitation of the back side of the film show a rise in photoconductivity (Figure 3a). Because of the short penetration depth (<100 nm) of the excitation light, the $\Delta T/T$ signal immediately after photoexcitation arises exclusively from the volume of the thin films in which light is absorbed and where the charge-carriers are initially concentrated. The THz probe beam on the other hand has a penetration depth much longer than the sample thickness and is detected in transmission geometry, therefore responding to mobile charge-carriers present anywhere within the full volume of the film. In consideration of the lower charge-carrier mobilities that we have observed in the quasi-2D region of the films, we can credit the rise in the OPTP dynamics following substrate-side photoexcitation to the transfer of charge-carriers from the low-mobility quasi-2D region to the higher-mobility 3D region. By analyzing the resulting photoconductivity enhancement, we are thus able to investigate the mechanisms underpinning such rapid transfer of charge-carriers.

Figure 3b schematically illustrates the mechanisms by which charge-carriers may be transferred from quasi-2D to 3D domains in the film. Here, we do not account for the transfer of excitons but rather focus on the movement of free charge-carriers. Although exciton transfer has been observed in layered perovskites,[26] it has been found to dominate at much shorter time scales (∼100 fs) and distances than we explore here and in the presence of higher exciton binding energies in strongly confined 2D layers, which are not present in our samples. We therefore focus on two main transfer mechanisms, which are diffusion of free charge-carriers and photon recycling.

The diffusion of free charge-carriers from the quasi-2D to the 3D domains will be aided by the slight downward slope in bandgap energy (Figure 3) and the strong gradient in charge-carrier density resulting from the short penetration depth of the photoexcitation, which will cause both electrons and holes

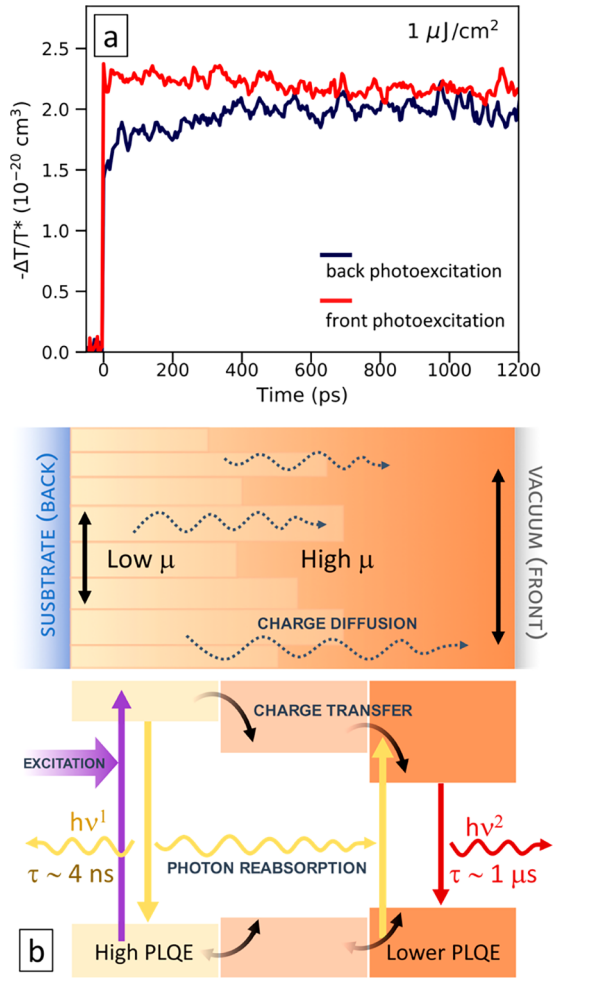

Figure 3. (a) OPTP dynamics measured with illumination incident on the front (red) or back (dark blue) side of the thin film, with fluence 1 μJ/cm^2. In order to account for different photoexcitation densities that result from the different reflectivity of the perovskite (front) or substrate (back) surfaces, the amplitudes have been plotted as $-\Delta T/T^* = (-\Delta T/T)/N_0$, where N_0 is the predicted initial density of photoexcited carriers (see Figure S6 for unnormalized data). (b) Schematic illustration of the charge-carrier transfer and recombination mechanisms operating in a thin metal halide perovskite film made of quasi-2D, higher bandgap domains near the substrate side, and a 3D, lower bandgap region near the front (vacuum) side.

to diffuse preferentially away from the illuminated area. As we discuss further below, given the measured values for charge-carrier mobilities, such diffusion should indeed occur within the nanosecond time scales of our observations. We note that because the photoconductivity probed by OPTP represents a sum of the electron and hole contributions, we cannot distinguish between the individual dynamics of electrons and holes. However, recent ultraviolet photoelectron spectroscopy (UPS)[9,34] measurements of quasi-2D lead iodide perovskites have revealed that the energetic positions of the valence band maxima (VBM) show little variation with layer thickness n, while the conduction band minima (CBM) show more pronounced steps, thus forming an energy cascade for electrons (see Figure 3). Therefore, while such a gradient in CBM will promote the transfer of electrons to lower-bandgap 3D domains toward the front side of our films, the alignment of the VBM should allow free movement of holes into any direction. Such hole transfer to higher band gap domains has

DOI: 10.1021/acs.nanolett.9b01242
Nano Lett. 2019, 19, 3953−3960

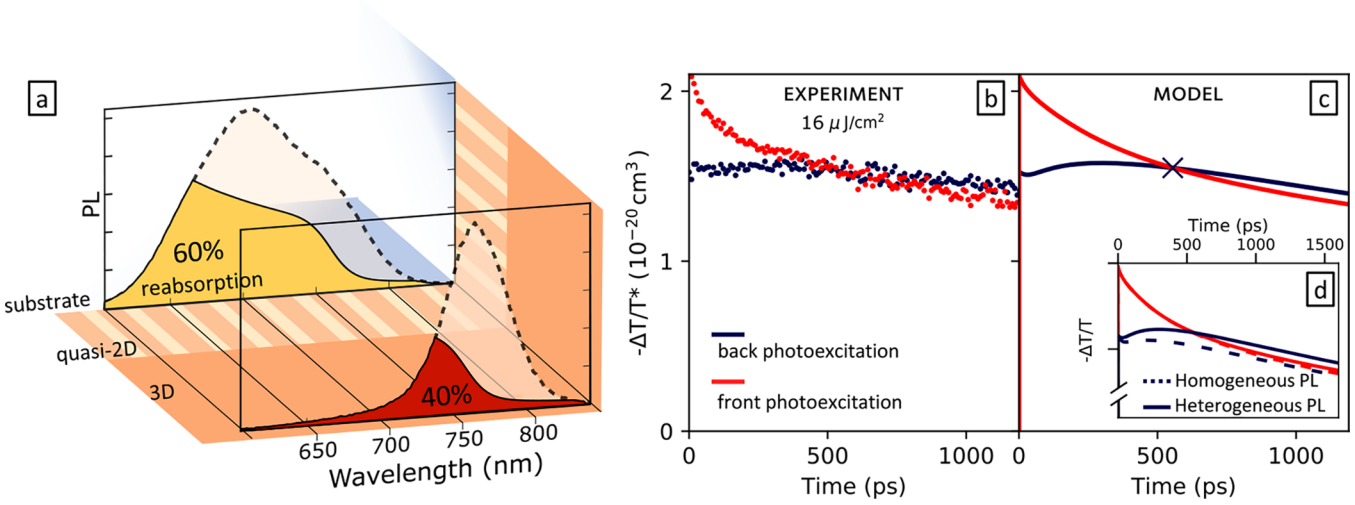

Figure 4. (a) PL spectra (dashed line, corrected for self-absorption) of the quasi-2D and 3D lead iodide perovskite regions of the thin film. The highlighted area indicates the spectral overlap with the absorption spectrum. The calculated photon recapture probabilities are 40% for 3D emission and 60% for quasi-2D emission. (b) OPTP dynamics measured with illumination incident on the front (red) or back (dark blue) side of the thin film, with fluence 16 μJ/cm^2. Dots represent experimental data and solid lines in (c) are simulated transients (accounting for charge diffusion and photon reabsorption under the assumption of heterogeneous PL emission; recombination rate constants were obtained from the fits to experimental data). (d) Simulated OPTP photoconductivity dynamics for photoexcitation incident on the front (red) or back (dark blue) of the thin film, both accounting for charge diffusion and photon reabsorption, but considering either homogeneous (dotted lines) or heterogeneous (solid lines) PL emission. In order to account for different photoexcitation densities that result from the different reflectivity of the perovskite (front) or substrate (back) surfaces, the amplitudes have been plotted as $-\Delta T/T^* = (-\Delta T/T)/N_0$, where N_0 is the predicted initial density of photoexcited carriers (see Figure S8 for unnormalized data). Simulated transients in (c,d) were obtained for a fixed value of N_0 on both sides (see Section S6 in Supporting Information for full details of the analysis).

indeed been previously observed by transient absorption spectroscopy.[26,35−37] This characteristic has important implications for solar cells fabricated with mixed-phase quasi-2D perovskites, as it allows for facile charge separation of electrons and holes toward opposite electrodes when a gradient of 2D effects through the depth profile is present.

The second effective mechanism for the transfer of charges that needs to be considered is the reabsorption of photons that have been emitted following radiative charge-carrier recombination. Such photon recycling is known to have significant effects on the excited state dynamics over the nanosecond time scale of our measurements.[38] As we show below, this process will be particularly efficient for the case of high-energy photons originating from the highly emissive quasi-2D domains, which have strong energetic overlap with the absorption spectrum of the lower-bandgap 3D perovskite.

To evaluate the relative importance of each of these mechanisms, we modeled the photoconductivity dynamics based on a modified version of our previously reported approach that accurately described the observed OPTP dynamics in 3D perovskite films.[38] As before, we account for the effects of the charge-carrier diffusion and photon reabsorption as well as carrier recombination,[38] but in addition now also consider the heterogeneous distribution of morphology and electronic properties through the film profile. Briefly, the initial charge-carrier population after a short pulse of photoexcitation is determined according to Beer's Law of absorption and decays exponentially away from the illuminated surface. At any given depth of the film, the carrier population evolves over time from its initial value, as a result of carrier recombination, carrier diffusion, and reabsorption of photons originating from radiative recombination that is tracked through the film. The mixed-phase morphology of the films, with the presence of both quasi-2D and 3D layers, requires us to account for the heterogeneous charge-carrier mobilities and spectral shape of PL emission. On the basis of film profilometry, STEM and spectroscopic data (see Section 4.1 in Supporting Information for details), we modeled the mixed-phase films as comprising two layers: one on the substrate side, consisting of a quasi-2D region of 150 nm thickness with effective mobility μ = 17.4 cm^2/(V s), on top of which resides a 3D perovskite layer with 300 nm thickness and μ = 23.9 cm^2/(V s) (Figure S9). The characteristic PL emission spectra associated with each layer were obtained from the PL spectra measured at early times after photoexcitation from either side (see insets in Figure 2b,e), which were corrected to account for self-absorption effects (Figure S12). A full description of the model is provided in Supporting Information.

Our model simulates the diffusion of charge-carriers based on the mobility and thickness of each layer and traces the photon reabsorption according to the absorption and PL spectra and the radiative rate. Simultaneously, the recombination rate constants are globally fitted to the fluence dependence of the experimental transients. First, we are able to determine the intrinsic value of the bimolecular recombination rate constant accurately from fits of the transients, shown in Figure 2c,f for both front and back photoexcitation and find a value similar to the one we have recently reported[38] for $MAPbI_3$ at room temperature (see Section S5 of the Supporting Information). Second, we are able to concentrate on a careful examination of the photoconductivity transients collected at lower excitation fluences to investigate the relative importance of the individual contribution of charge diffusion and photon reabsorption. Figure 4b shows an example for such transients, which exhibit a slow rise in photoconductivity for excitation from the back side (quasi-2D region) but a decay for excitation from the front side (3D layer). In the former case, importantly, initial excitation of the quasi-2D region leads to a

DOI: 10.1021/acs.nanolett.9b01242
Nano Lett. 2019, 19, 3953−3960

crossing in the photoconductivity transient at later times. This observation is surprising, given that for similar charge recombination rates the redistribution of charge-carriers would eventually result in a uniform population throughout the film giving equivalent photoconductivity regardless of where carries are initially photoexcited. Alternatively, higher radiative losses in quasi-2D domains could ultimately result in lower photoconductivity values. However, such crossing in the dynamics instead shows that the photoconductivity attained at long times after excitation of the 2D phase exceeds that observed for direct excitation of the 3D phase. To understand the origin of this enhancement of photoconductivity and the relative contributions of charge-carrier diffusion and photon reabsorption, we applied the model to fit these transients with either or both of these mechanisms omitted.

Focusing first on the differences in the OPTP transients observed at early times, we find that exclusion of photon reabsorption from the dynamical model still allows us to reproduce the dynamics with good accuracy (see Figures S13 and S14). Charge diffusion from quasi-2D domains with lower carrier mobility to the high-mobility 3D region therefore appears to be the main mechanism influencing the early transient enhancement of the photoconductivity following excitation of the quasi-2D region. We observed that such a rise cannot be reproduced when only photon reabsorption is used to redistribute carriers across the film. However, when considering both mechanisms, reabsorption results in prolonged charge-carrier lifetimes and a further enhancement of photoconductivity at later times with respect to the effect of diffusion alone (see Section S6.2 in Supporting Information).

Finally, we are able to relate the crossing of the transients observed at elevated excitation fluences (Figure 4b) for front and back excitation to the heterogeneous nature of the PL emission spectra in these films. We observed that such crossing can only be reproduced when accounting for photon reabsorption. We then evaluate how the sample heterogeneity affects the efficiency of photon recapture. Here, we simulated the OPTP dynamics incorporating both charge diffusion and photon reabsorption, but now consider two different spectral scenarios for photon reabsorption. In the first case, we considered heterogeneous PL, where the emission of the quasi-2D region has two components centered at 1.59 and 1.74 eV (as derived from back-surface excitation spectra) whereas the emission of the 3D region is centered at 1.59 eV (as illustrated in Figure 4a). In the second case, we considered homogeneous PL across the film, that is, both regions exhibit emission centered at 1.59 eV (spectral shape of 3D $MAPbI_3$, as observed for front-surface excitation), and its overlap with the absorption spectrum of the film that is dominated by 3D $MAPbI_3$ near the onset (Figure 1c). As Figure 4a illustrates, for the case of heterogeneous PL the high energy photons emitted by the quasi-2D domains overlap much better with the absorption coefficient spectrum of the 3D domains, resulting in a 60% probability of photon recapture, compared with a 40% probability for the case of 3D $MAPbI_3$ emission (see Section S6.2.1 in Supporting Information for full details of calculation). Such improved spectral overlap between absorption and emission enables the quasi-2D PL emission to contribute to a stronger enhancement of photoconductivity over time (Figure S21) as a consequence of more efficient photon reabsorption by the 3D $MAPbI_3$ layer. As Figure 4d shows, the modeled OPTP transients for front photoexcitation (red) and back photoexcitation (dark blue) will only cross at later times if heterogeneous PL is considered at this fluence, whereas they approach each other at long times for the case of homogeneous PL. The experimentally observed crossing of these transients (Figure 4b) thus provides clear evidence that photon reabsorption, boosted by the higher-energy emission of the quasi-2D region, augments capture and retention of charge-carriers in the 3D perovskite layer.

Our modeling of photon reabsorption effects in these mixed-phase perovskite films thus reveals two favorable effects. First, we find that photon recapture minimizes radiative losses, even when charge-carriers recombine relatively rapidly in the quasi-2D phase of the material, because of efficient photon recapture that prolongs the effective charge-carrier lifetime. As a second effect, photon reabsorption leads to somewhat faster redistribution of charge-carriers from quasi-2D to 3D domains than would be expected from charge diffusion alone. These two effects are able to compensate, respectively, the increased charge-carrier recombination rate and reduced mobility that characterize quasi-2D perovskites. Because radiative recombination is a bimolecular process, photon reabsorption appears to affect the dynamics more strongly at higher excitation fluences (Figure S7). At low excitation fluences, charge-carrier diffusion is the dominant mechanism and the measured THz photoconductivity reaches the same amplitude for both front and back excitation (Figure 3a), because the charge-carrier density becomes evenly spread through the film which compensates for the differences in charge mobilities between regions of the film. At higher fluences (Figure 4b), on the other hand, the contribution of radiative recombination increases, making photon reabsorption particularly effective and leading to the observed crossing of transients. Therefore, at the radiative limit the more highly optimized photon reabsorption resulting from better spectral overlap between the quasi-2D emission and the 3D perovskite absorption ultimately results in slightly longer charge-carrier lifetimes and increased photoconductivity when the quasi-2D side is illuminated. We also note that the efficiency of photon recapture is not greatly affected by the total thickness of the film for values typically implemented in perovskite solar cells (see Section 6.3 in the Supporting Information). This boost in lifetime and photoconductivity promoted by the higher PL energy of the quasi-2D phase suggests that light-harvesting devices fabricated with such mixed-phase perovskite films could benefit from illumination being incident on the side containing the quasi-2D material. In addition, we note that the presence of quasi-2D domains should contribute to a decrease of nonradiative losses. The passivation of grain boundaries by the large organic cation can decrease the trap-assisted recombination rates, whereas the high radiative rates in the quasi-2D domains result in higher PL quantum efficiencies.[7,9] Therefore, the heterogeneous photon recycling we observe here will be particularly effective.

In conclusion, we have investigated the charge-carrier transport in lead iodide perovskite films with a self-assembled graded structure comprising quasi-2D domains on the substrate side, topped with a layer of 3D $MAPbI_3$. We find that, as expected, the presence of electronic confinement results in lower charge-carrier mobility and significantly higher radiative recombination rates. However, through analysis of the photoconductivity dynamics following photoexcitation, we show why these effects still present no obstacle to the implementation of these materials in photovoltaic cells. First, the rapid diffusion of charge carriers to 3D perovskite domains with higher charge-carrier mobility leads to a strong recovery

DOI: 10.1021/acs.nanolett.9b01242
Nano Lett. 2019, 19, 3953−3960

of photoconductivity in the semiconductor even after initial illumination of mostly the quasi-2D material. Second, the efficient reabsorption of photons originating from charge-carrier recombination inside the quasi-2D domains results in a further boost in photoconductivity associated with prolonged charge-carrier lifetimes. Such heterogeneous photon recycling is particularly effective because the emission spectrum of the quasi-2D domains is blue-shifted beyond the absorption onset of the 3D perovskite. Thus, the effects of charge diffusion and photon recycling are able to compensate for the less favorable aspects of dielectric confinement for the graded structures under investigation here. Such morphologies may therefore offer the best of both worlds, combining enhanced moisture resistance and surface passivation through the incorporation of the large hydrophobic cations with excellent charge transporting properties needed for highly efficient solar cells.

■ ASSOCIATED CONTENT

Supporting Information

The Supporting Information is available free of charge on the ACS Publications website at DOI: 10.1021/acs.nanolett.9b01242.

Material preparation; structural and optical characterization data; experimental details of OPTP and PL setups, description of charge-carrier dynamics model; analysis of the effects of charge-carrier diffusion, photon reabsorption, and quasi-2D layer thickness on OPTP transients (PDF)

■ AUTHOR INFORMATION

Corresponding Authors

*E-mail: iamjpwang@njtech.edu.cn.
*E-mail: laura.herz@physics.ox.ac.uk.

ORCID

Michael B. Johnston: 0000-0002-0301-8033
Jianpu Wang: 0000-0002-2158-8689
Laura M. Herz: 0000-0001-9621-334X

Notes

The authors declare no competing financial interest.

■ ACKNOWLEDGMENTS

The authors gratefully acknowledge financial support from the Engineering and Physical Sciences Research Council (U.K.) (EPSRC), the European Union's Horizon 2020 research and innovation programme under the Marie Skłodowska-Curie grant agreement No. 675867 (INFORM), the Joint Research Program between China and the European Union (2016YFE0112000), and the National Natural Science Foundation of China (91733302, 61725502).

■ REFERENCES

(1) NREL. Best Research-Cell Efficiencies https://www.nrel.gov/pv/assets/images/efficiency-chart.png (accessed May 23, 2018).
(2) Yang, J.; Siempelkamp, B. D.; Liu, D.; Kelly, T. L. *ACS Nano* **2015**, *9* (2), 1955−1963.
(3) Huang, J.; Tan, S.; Lund, P.; Zhou, H. *Energy Environ. Sci.* **2017**, *10* (11), 2284−2311.
(4) Christians, J. A.; Miranda Herrera, P. A.; Kamat, P. V. *J. Am. Chem. Soc.* **2015**, *137* (4), 1530−1538.
(5) Smith, I. C.; Hoke, E. T.; Solis-Ibarra, D.; McGehee, M. D.; Karunadasa, H. I. *Angew. Chem., Int. Ed.* **2014**, *53* (42), 11232−11235.
(6) Yang, R.; Li, R.; Cao, Y.; Wei, Y.; Miao, Y.; Tan, W. L.; Jiao, X.; Chen, H.; Zhang, L.; Chen, Q.; et al. *Adv. Mater.* **2018**, *30*, 1804771.
(7) Milot, R. L.; Sutton, R. J.; Eperon, G. E.; Haghighirad, A. A.; Martinez Hardigree, J.; Miranda, L.; Snaith, H. J.; Johnston, M. B.; Herz, L. M. *Nano Lett.* **2016**, *16* (11), 7001−7007.
(8) Even, J.; Pedesseau, L.; Katan, C. *ChemPhysChem* **2014**, *15* (17), 3733−3741.
(9) Yuan, M.; Quan, L. N.; Comin, R.; Walters, G.; Sabatini, R.; Voznyy, O.; Hoogland, S.; Zhao, Y.; Beauregard, E. M.; Kanjanaboos, P.; et al. *Nat. Nanotechnol.* **2016**, *11* (10), 872−877.
(10) Sun, Y.; Zhang, L.; Wang, N.; Zhang, S.; Cao, Y.; Miao, Y.; Xu, M.; Zhang, H.; Li, H.; Yi, C.; et al. *npj Flex. Electron.* **2018**, *2* (1), 12.
(11) Wang, N.; Cheng, L.; Ge, R.; Zhang, S.; Miao, Y.; Zou, W.; Yi, C.; Sun, Y.; Cao, Y.; Yang, R.; et al. *Nat. Photonics* **2016**, *10* (11), 699−704.
(12) Chin, X. Y.; Perumal, A.; Bruno, A.; Yantara, N.; Veldhuis, S. A.; Martínez-Sarti, L.; Chandran, B.; Chirvony, V.; Lo, A. S. Z.; So, J.; et al. *Energy Environ. Sci.* **2018**, *11* (7), 1770−1778.
(13) Zheng, H.; Liu, G.; Zhu, L.; Ye, J.; Zhang, X.; Alsaedi, A.; Hayat, T.; Pan, X.; Dai, S. *Adv. Energy Mater.* **2018**, *8* (21), 1800051.
(14) Cao, D. H.; Stoumpos, C. C.; Farha, O. K.; Hupp, J. T.; Kanatzidis, M. G. *J. Am. Chem. Soc.* **2015**, *137* (24), 7843−7850.
(15) Tsai, H.; Nie, W.; Blancon, J. C.; Stoumpos, C. C.; Asadpour, R.; Harutyunyan, B.; Neukirch, A. J.; Verduzco, R.; Crochet, J. J.; Tretiak, S.; et al. *Nature* **2016**, *536* (7616), 312−317.
(16) Zhang, X.; Ren, X.; Liu, B.; Munir, R.; Zhu, X.; Yang, D.; Li, J.; Liu, Y.; Smilgies, D. M.; Li, R.; et al. *Energy Environ. Sci.* **2017**, *10* (10), 2095−2102.
(17) Zhou, N.; Shen, Y.; Li, L.; Tan, S.; Liu, N.; Zheng, G.; Chen, Q.; Zhou, H. *J. Am. Chem. Soc.* **2018**, *140* (1), 459−465.
(18) Tsai, H.; Asadpour, R.; Blancon, J. C.; Stoumpos, C. C.; Even, J.; Ajayan, P. M.; Kanatzidis, M. G.; Alam, M. A.; Mohite, A. D.; Nie, W. *Nat. Commun.* **2018**, *9* (1), 2130.
(19) Wang, Z.; Lin, Q.; Chmiel, F. P.; Sakai, N.; Herz, L. M.; Snaith, H. J. *Nat. Energy* **2017**, *2* (9), 17135.
(20) Quan, L. N.; Yuan, M.; Comin, R.; Voznyy, O.; Beauregard, E. M.; Hoogland, S.; Buin, A.; Kirmani, A. R.; Zhao, K.; Amassian, A.; et al. *J. Am. Chem. Soc.* **2016**, *138* (8), 2649−2655.
(21) Straus, D. B.; Hurtado Parra, S.; Iotov, N.; Gebhardt, J.; Rappe, A. M.; Subotnik, J. E.; Kikkawa, J. M.; Kagan, C. R. *J. Am. Chem. Soc.* **2016**, *138* (42), 13798−13801.
(22) Neutzner, S.; Thouin, F.; Cortecchia, D.; Petrozza, A.; Silva, C.; Srimath Kandada, A. R. *Phys. Rev. Mater.* **2018**, *2* (6), No. 064605.
(23) Thouin, F.; Valverde-Chávez, D. A.; Quarti, C.; Cortecchia, D.; Bargigia, I.; Beljonne, D.; Petrozza, A.; Silva, C.; Srimath Kandada, A. R. *Nat. Mater.* **2019**, *18* (4), 349−356.
(24) Liu, J.; Leng, J.; Wu, K.; Zhang, J.; Jin, S. *J. Am. Chem. Soc.* **2017**, *139* (4), 1432−1435.
(25) Chen, P.; Meng, Y.; Ahmadi, M.; Peng, Q.; Gao, C.; Xu, L.; Shao, M.; Xiong, Z.; Hu, B. *Nano Energy* **2018**, *50*, 615−622.
(26) Proppe, A. H.; Elkins, M. H.; Voznyy, O.; Pensack, R. D.; Zapata, F.; Besteiro, L. V.; Quan, L. N.; Quintero-Bermudez, R.; Todorovic, P.; Kelley, S. O.; et al. *J. Phys. Chem. Lett.* **2019**, *10*, 419−426.
(27) Wehrenfennig, C.; Liu, M.; Snaith, H. J.; Johnston, M. B.; Herz, L. M. *J. Phys. Chem. Lett.* **2014**, *5* (8), 1300−1306.
(28) Mao, L.; Tsai, H.; Nie, W.; Ma, L.; Im, J.; Stoumpos, C. C.; Malliakas, C. D.; Hao, F.; Wasielewski, M. R.; Mohite, A. D.; et al. *Chem. Mater.* **2016**, *28* (21), 7781−7792.
(29) Blancon, J. C.; Tsai, H.; Nie, W.; Stoumpos, C. C.; Pedesseau, L.; Katan, C.; Kepenekian, M.; Soe, C. M. M.; Appavoo, K.; Sfeir, M. Y.; et al. *Science (Washington, DC, U. S.)* **2017**, *355* (6331), 1288−1292.
(30) Tsai, H.; Nie, W.; Blancon, J. C.; Stoumpos, C. C.; Asadpour, R.; Harutyunyan, B.; Neukirch, A. J.; Verduzco, R.; Crochet, J. J.; Tretiak, S.; et al. *Nature* **2016**, *536* (7616), 312−317.
(31) Wehrenfennig, C.; Eperon, G. E.; Johnston, M. B.; Snaith, H. J.; Herz, L. M. *Adv. Mater.* **2014**, *26* (10), 1584−1589.
(32) Herz, L. M. *ACS Energy Lett.* **2017**, *2* (7), 1539−1548.

DOI: 10.1021/acs.nanolett.9b01242
Nano Lett. 2019, 19, 3953−3960

(33) Johnston, M. B.; Herz, L. M. *Acc. Chem. Res.* **2016**, *49* (1), 146−154.
(34) Cao, D. H.; Stoumpos, C. C.; Farha, O. K.; Hupp, J. T.; Kanatzidis, M. G. *J. Am. Chem. Soc.* **2015**, *137* (24), 7843.
(35) Liu, J.; Leng, J.; Wu, K.; Zhang, J.; Jin, S. *J. Am. Chem. Soc.* **2017**, *139* (4), 1432−1435.
(36) Shang, Q.; Wang, Y.; Zhong, Y.; Mi, Y.; Qin, L.; Zhao, Y.; Qiu, X.; Liu, X.; Zhang, Q. *J. Phys. Chem. Lett.* **2017**, *8* (18), 4431−4438.
(37) Proppe, A. H.; Quintero-Bermudez, R.; Tan, H.; Voznyy, O.; Kelley, S. O.; Sargent, E. H. *J. Am. Chem. Soc.* **2018**, *140* (8), 2890−2896.
(38) Crothers, T. W.; Milot, R. L.; Patel, J. B.; Parrott, E. S.; Schlipf, J.; Müller-Buschbaum, P.; Johnston, M. B.; Herz, L. M. *Nano Lett.* **2017**, *17* (9), 5782−5789.

DOI: 10.1021/acs.nanolett.9b01242
Nano Lett. 2019, 19, 3953−3960